ROYAL SOCIETY
OF CHEMISTRY

PAPER

Check for updates

Ultrasound-based mechanochemical generation of reactive oxygen species from nanoparticle-conjugated amyloid fibrils†

Soumi Das, Jayanta Dolai, [ID] * Buddhadev Mukherjee, Anupam Maity [ID] * and Nikhil R. Jana [ID] *

Piezoelectric biomaterials have diverse potential biomedical applications *via* ultrasound-based wireless mechanochemical reaction at a remote area of the body/medical device. However, most biomaterials have weak piezoelectric properties compared to chemically designed piezoelectric materials. In the current approach, piezoelectric properties of certain biomaterials are enhanced by transforming them into anisotropic fibril/sheet-like morphology. Here, we demonstrate that the piezoelectric property of amyloid fibrils can be enhanced by 2 times *via* conjugation with nanoparticles and this can enhance the ultrasound-based mechanochemical production of reactive oxygen species by 4 times. In particular, we have synthesized nanoparticle-conjugated lysozyme fibrils with a piezoelectric constant value as high as 82 pm V^{-1}. Thin films derived from these materials can generate periodic voltage/current pulses under the exposure of medical-grade ultrasound that can reach up to 1 V/15 nA. A colloidal dispersion of these materials generates superoxide/hydroxyl radicals *via* ultrasound-based mechanochemical reaction and degrade a dye. This strategy can be adapted to improve the mechanochemical reaction performance of weakly piezoelectric materials.

Introduction

Piezoelectric materials produce electric charge in response to applied mechanical stress.[1,2] Inorganic nanocrystals that lack a center of symmetry such as ZnO, PbZrO$_3$, BaTiO$_3$, and ZnSnO$_3$, are classic example of piezoelectric nanomaterials.[3,4] These materials have diverse potential biomedical applications including drug delivery, tissue engineering, tumor therapy, biosensors and curing of neurodegenerative disease.[5–7] However, the cytotoxicity of many of these inorganic nanomaterials restricts their biomedical applications, as their interaction with biological systems can induce harmful side effects.[5] In this context, biomolecule-based piezoelectric materials are envisioned for advanced biomedical applications due to their biocompatibility and flexibility.[8–10] Bone, silk, wood, collagen, tendon, and deoxyribonucleic acid (DNA) films are notable examples of naturally occurring piezoelectric biomaterials.[11–15] The piezoelectricity exhibited by these biological components is believed to play a crucial role in

School of Materials Science, Indian Association for the Cultivation of Science, 2A & 2B Raja S. C. Mullick Road, Kolkata-700032, India. E-mail: intjd2@iacs.res.in; rajamaity90@gmail.com; camnrj@iacs.res.in

† Electronic supplementary information (ESI) available: Synthesis details of amyloid fibrils and nanoparticle composites with amyloid fibrils, experimental procedure for ultrasound-based mechanochemical reaction and additional materials characterization data. See DOI: https://doi.org/10.1039/d5mr00041f

maintaining physiological balance in living systems and is closely linked to human health.[10] For example, the piezoelectricity of skin is responsible for converting mechanical stress into electrical signals, which helps in sensory perception. This property also aids in the regulation of various physiological processes by providing feedback on touch and pressure.[13] Additionally, it contributes to the skin's ability to heal and regenerate by influencing cellular activities.[13] Certain amino acids, proteins and polypeptides also exhibit piezoelectricity.[11,12] The anisotropic morphology of fibers and fibrils derived from specific amino acids, peptides, and proteins also exhibits piezoelectric properties.[16] For example, fibrils derived from lysozyme, fluorenyl methyl oxy carbonyl diphenylalanine (Fmoc-FF), and cyclic β-peptides showcase piezoelectric properties.[17–19] When piezoelectric materials are exposed to ultrasound-based mechanical stress, they generate electric charge and trigger redox reactions with water and dissolved oxygen. This process leads to mechanochemical formation of reactive oxygen species (ROS), such as hydroxyl radicals (˙OH), superoxide radicals (O$_2$˙$^-$) and hydrogen peroxide (H$_2$O$_2$).[20–22] These generated ROS are used for pollutant degradation, chemical conversion and functional group transformation.[20–22] These processes are commonly called piezocatalysis. Considering the weak piezoelectric properties of biomaterials, various approaches have been adapted for enhancing piezocatalysis that include increased structural anisotropy or composite formation with nanoparticles/polymers.[18,23,24] These approaches

offer a more asymmetric arrangement of charges,[18,23] lower the charge recombination processes[23] and induce greater imbalance of charge carriers on the surface of these materials.[23]

We have recently demonstrated that the piezoelectric property of amyloid/protein fibrils can be enhanced by 4–10 times *via* extension of the β-sheet structure with piezoelectric constant values in the range of 24–42 pm V^{-1} for fibrils and values up to 62 pm V^{-1} for sheet/bundle-like structures.[18] Considering the fact that amyloid/protein fibrils can be routinely made *in vitro* with good colloidal properties, further enhancement of their piezoelectric properties can be beneficial from an application point of view. In this context, we have investigated the piezoelectric property of nanoparticle-conjugated amyloid fibrils. We demonstrate that the piezoelectric property of amyloid fibrils can be enhanced by 2 times *via* conjugation with nanoparticles and the piezoelectric constant value can reach up to 82 pm V^{-1}. This enhanced piezoelectric property is shown to enhance ultrasound-based mechanochemical reactions by 4 times.

Results and discussion

Nanoparticle attachment enhances the piezoelectric property of amyloid fibril

We have selected lysozyme fibrils as a model amyloid fibril as these and their nanoparticle composites are well studied[25] (Fig. 1a). Lysozyme protein-based amyloid fibrils have been synthesized using our previously reported method.[18] Silica-coated hydrophilic Fe$_3$O$_4$ nanoparticles and histidine-coated Au nanoparticles are separately synthesized following reported methods.[23,26] Gold nanoparticles are selected due to the well-known property of enhancing photocatalytic processes *via* lowering of charge carrier recombination[27] and iron oxide nanoparticles are selected due to their well-known Fenton reaction property.[28] Transmission electron microscopy (TEM) of these nanoparticles shows a spherical shape with a core size of

5–8 nm (see ESI, Fig. S1†). Next, nanoparticle composites are prepared by simple mixing of a colloidal dispersion of nanoparticles with a colloidal dispersion of amyloid fibrils under stirring conditions (Fig. 1a). TEM images show fibril morphology and attachment of Au/Fe$_3$O$_4$ nanoparticles (Fig. 1b–e, and ESI, Fig. S2†). Such attachment is due to the interaction between the zwitterionic surface charge of the fibrils and the cationic surface charge of the metal/metal oxide nanoparticles. X-ray diffraction (XRD) patterns of the composites demonstrate the presence of characteristic reflections for Au/Fe$_3$O$_4$ nanoparticles (ESI, Fig. S3†).

Next, we have investigated the piezoelectric property of amyloid fibrils after composite formation with nanoparticles *via* piezoresponse force microscopy (PFM) (Fig. 2). The characteristic butterfly loop of amplitude *versus* bias voltage, along with the phase hysteresis plot, indicates the presence of piezoelectric properties. The slope of the amplitude *versus* bias voltage loop is used to calculate the piezoelectric constant of the samples.[23,24,29] The piezoelectric constants of amyloid fibrils and amyloid–Au and amyloid–Fe$_3$O$_4$ composites are found to be 41 pm V^{-1}, 76 pm V^{-1} and 82 pm V^{-1}, respectively. It is worth mentioning that attachment of nanoparticles on amyloid fibrils results in 2 times enhancement of the piezoelectric constant. Such enhancement is likely due to a combination of enhanced imbalance of surface charge along the elongated polar axis and the charge reservoir property of metal/metal oxide nanoparticles.[23,24,29]

To gain a deeper understanding of the microstructure-dependent polarization of amyloid fibrils and their composites, the dielectric permittivity has been studied (ESI, Fig. S4†). Since the dielectric and piezoelectric properties are closely related, an insightful investigation of the frequency-dependent dielectric permittivity is conducted. The dielectric constant (ε') of the investigated samples was estimated using the following relation:
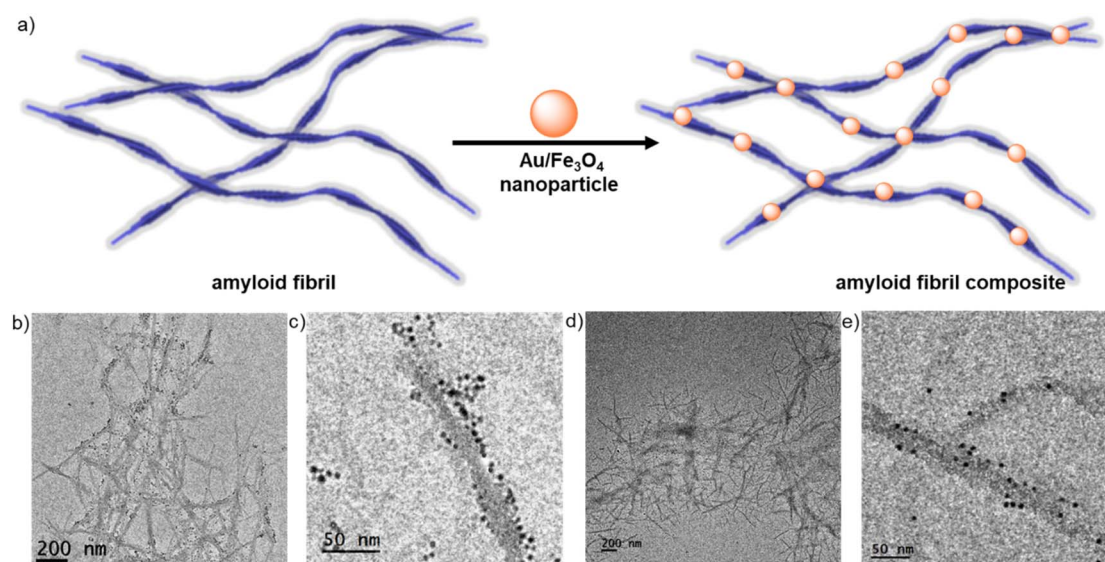

Fig. 1 (a) Schematic representation of amyloid fibrils and their gold/iron oxide composites. TEM images of amyloid–Au (b and c) and amyloid–Fe$_3$O$_4$ (d and e) composites. The magnified images demonstrate the attachment of Au/Fe$_3$O$_4$ nanoparticles with amyloid fibrils.
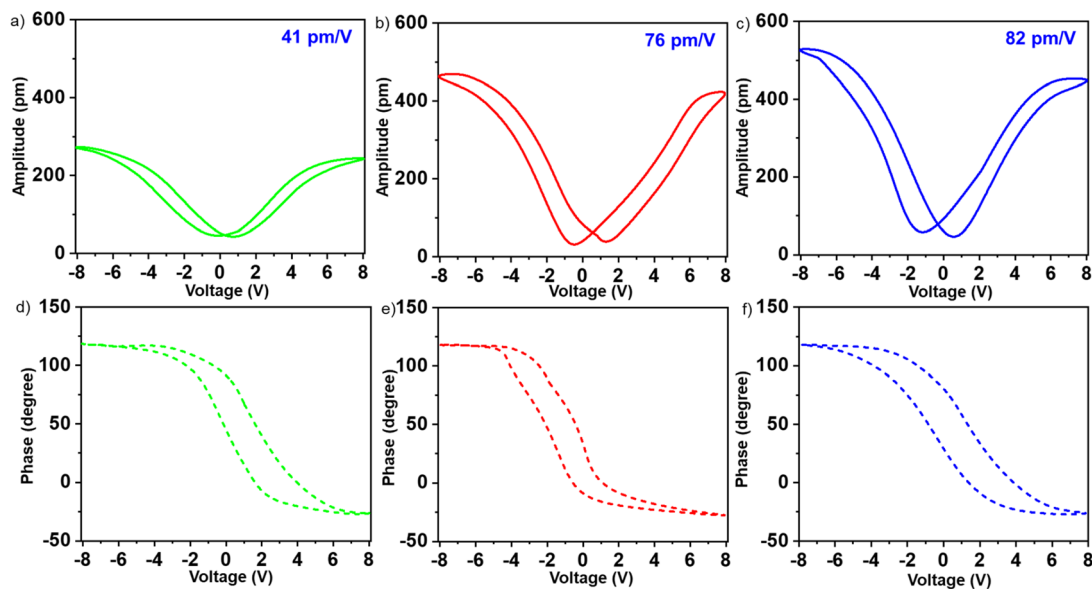
Fig. 2 Amplitude-voltage butterfly loops of amyloid fibril (a), amyloid–Au (b) and amyloid–Fe$_3$O$_4$ (c) with piezoelectric constant values shown as insets. Phase hysteresis loops of amyloid fibril (d), amyloid–Au (e) and amyloid–Fe$_3$O$_4$ (f).
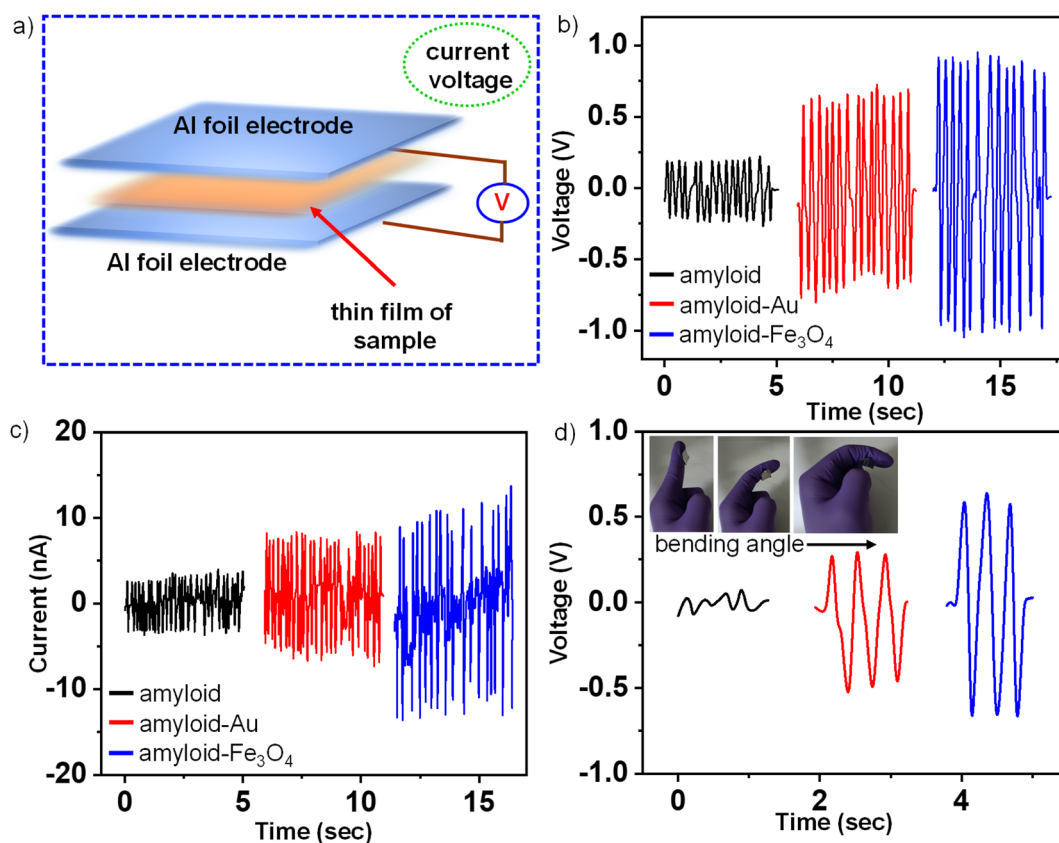

Fig. 3 (a) Schematic representation of the experimental setup for piezo-current and piezo-voltage measurement. Piezoelectric response of amyloid fibrils and their composites measured using mechanical stress: (b) piezo-voltage and (c) piezo-current. (d) Piezo-voltage response patterns of the amyloid–Fe$_3$O$_4$ composite sensor fixed on a finger under different bending angles.
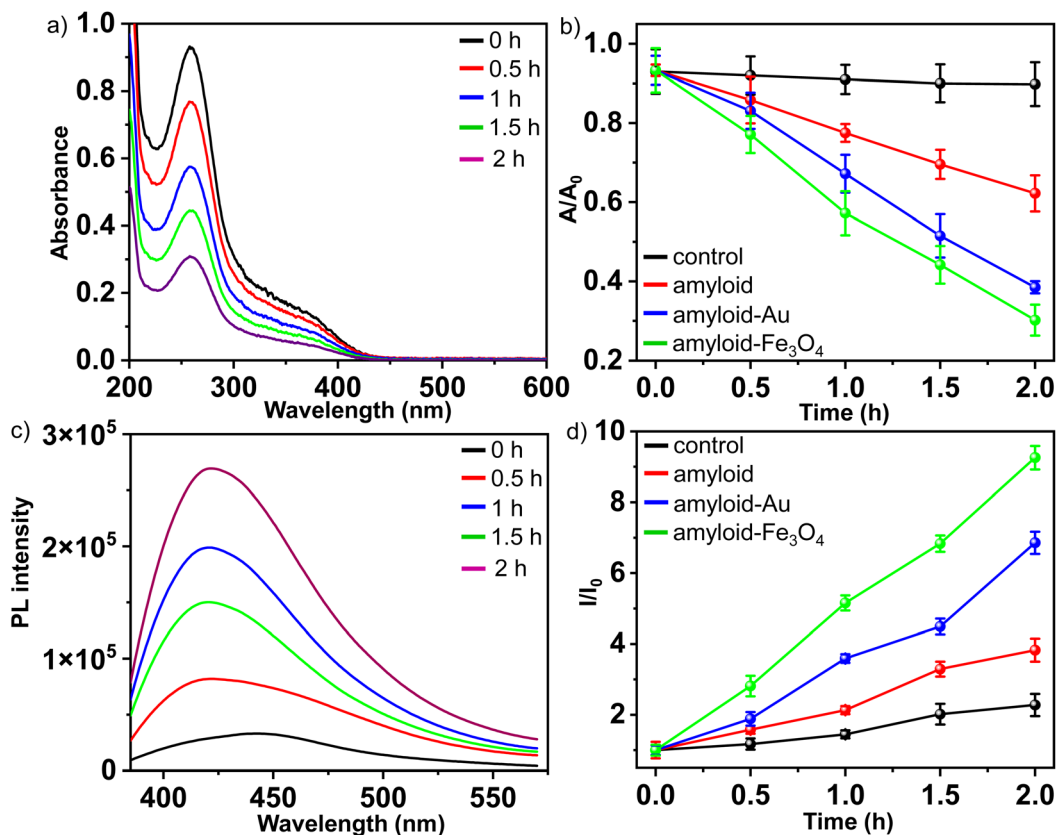
Fig. 4 Evidence of ROS generation by colloidal amyloid fibrils and their composites (1 mg mL^{-1}) under ultrasound exposure. (a) NBT absorbance-based detection of superoxide radicals produced by the amyloid–Fe$_3$O$_4$ composite, which decreases with ultrasound exposure time. (b) Enhanced superoxide radical generation by amyloid fibrils after composite formation with nanoparticles. Here, A/A_0 is the ratio of the absorbance of NBT after and before ultrasound exposure. (c) Terephthalic acid emission-based detection of hydroxyl radicals produced by the amyloid–Fe$_3$O$_4$ composite, which increases with ultrasound exposure time. (d) Enhanced hydroxyl radical generation by amyloid fibrils after composite formation with nanoparticles. Here, I/I_0 is the ratio of the fluorescence intensity of terephthalic acid after and before ultrasound exposure. An ultrasonic transducer with 120 W power and 33 kHz frequency is used for all of these measurements. Each error bar represents the mean of three independent experiments.

$$\varepsilon' = (Ct)/(\varepsilon_0 A),$$

where A, t, and C denote the area, thickness, and capacitance of the sample, respectively, and $\varepsilon_0 \sim 8.85 \times 10^{-12}$ F m^{-1} (free-space permittivity). Results show that the amyloid–Fe$_3$O$_4$ composite exhibits a higher dielectric constant than the amyloid–Au composite followed by amyloid fibrils.

We have further measured the open circuit voltage and short circuit current of thin-film samples under applied mechanical stress (Fig. 3a, ESI, Fig. S5†). The current/voltage measurements clearly show the appearance of positive and negative peaks that correspond to the immediate response to the applied stress and the material's damping effect, respectively, demonstrating the piezoelectric characteristics of the films. The obtained electrical output for amyloid fibrils and their composites is closely related to their piezoelectric constant values, and the amyloid–Fe$_3$O$_4$ generates the maximum voltage (about 1 V) and maximum current (about 15 nA), followed by amyloid–Au and amyloid fibril (Fig. 3b,c). We have further investigated the application potential of the amyloid-Fe$_3$O$_4$ composite as a human motion sensor. As shown in Fig. 3d, the sensor is attached to a finger.

When the finger is bent from a relaxed state to a specific angle, piezoelectric signals are generated and the voltage is amplified with increasing angle. These results demonstrate that amyloid fibril-based composites have significant potential for monitoring human motion and enabling various practical self-powered sensing applications in medical devices.

Enhancement of mechanochemical ROS generation by amyloid fibrils after nanoparticle attachment

Next, we have investigated the mechanochemical reaction performance of amyloid fibrils and their nanocomposites using ultrasound. Ultrasound is a unique source in generating periodic mechanical pressure and, more importantly, it is used in different medical/therapeutic applications.[5–7] Piezoelectric materials can generate an electric charge when subjected to stress, such as ultrasound. These electrical charges induce redox reactions with water and dissolved oxygen to produce ROS. In this case we have examined the generation of ROS such as hydroxyl radicals ($^{\bullet}$OH) and superoxide radicals ($O_2^{\bullet-}$), induced by ultrasound (Fig. 4). Typically, a colloidal dispersion of amyloid fibrils or their nanocomposite is mixed with
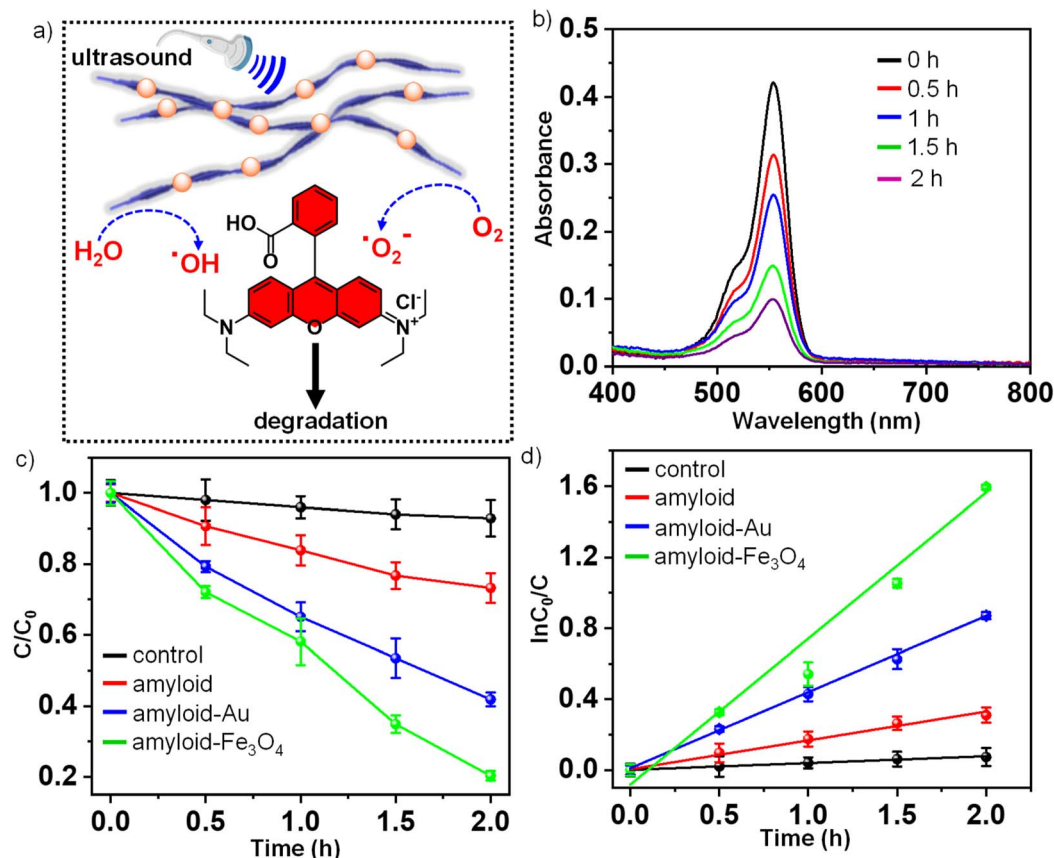
Fig. 5 (a) Schematic representation of rhodamine B degradation using an amyloid fibril-based colloidal nanocomposite. (b) Rhodamine B degradation by the amyloid−Fe$_3$O$_4$ composite in the presence of ultrasound exposure as observed by a progressive decrease of rhodamine B absorbance. (c) Rhodamine B degradation kinetics in the presence of amyloid fibrils and their composites with nanoparticles. Control represents the degradation of rhodamine B with ultrasound. (d) Plot of ln(C_0/C) vs. time using different piezocatalysts. An ultrasonic transducer with 120 W power and 33 kHz frequency is used for all of these measurements. Each error bar represents the mean of three independent experiments.

terephthalic acid (probe for hydroxyl radicals) or nitroblue tetrazolium (NBT) (probe for superoxide radicals) and exposed to ultrasound. Next, a part of the reaction mixture is collected at

different time points for spectroscopic investigation (Fig. 4a–d). Hydroxyl radicals react with terephthalic acid, leading to the generation of fluorescent 2-hydroxyterephthalic acid (ex:
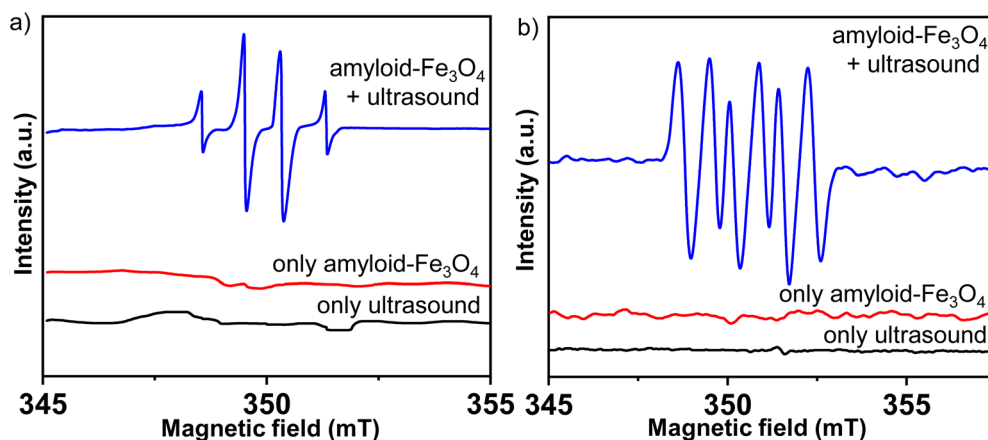

Fig. 6 ESR spectra of DMPO-trapped ROS species generated by the amyloid−Fe$_3$O$_4$ composite under ultrasonic vibration. Four characteristic signature peaks (1 : 1 : 1 : 1) of DMPO-O$_2$·⁻ adduct in DMSO solvent (a) and four characteristic signature peaks (1 : 2 : 2 : 1) of DMPO-·OH adduct in water solvent (b) suggest the formation of superoxide/hydroxyl radicals. Control experiments show that in the absence of ultrasound or in the absence of amyloid−Fe$_3$O$_4$ these ROS cannot be produced.

315 nm, em: 420–430 nm).[21] The increase in emission intensity with ultrasound exposure time is used to quantify the level of hydroxyl radicals generated under the piezocatalytic condition (Fig. 4). Superoxide radicals react with NBT, leading to a decrease in the UV-visible absorption peak of NBT at 259 nm due to the production of an insoluble bright blue formazan product.[21] The decrease in absorbance with increasing ultrasound exposure time is utilized to quantify the level of superoxide radicals under the piezocatalytic condition (Fig. 4). We note three distinct observations. First, the ROS generation capability of amyloid fibrils increases significantly after the attachment of gold/Fe_3O_4 nanoparticles and Fe_3O_4 nanoparticles offer better enhancement of mechanochemical ROS generation (Fig. 4a–d). Both assays indicate that the amyloid–Fe_3O_4 composite generates the highest amount of hydroxyl and superoxide radicals, followed by the amyloid–Au composite and amyloid fibrils, under similar experimental conditions. Control experiments indicate that either ultrasound alone or Au/Fe_3O_4 nanoparticles generate only a minimal amount of ROS under similar experimental conditions (ESI, Fig. S6†).

Second, there is a correlation between piezoelectric constant and mechanochemically generated ROS. It is expected that a higher piezoelectric constant would enhance charge migration, thereby improving mechanochemical ROS generation performance.[24] Hence, the amyloid–Fe_3O_4 composite with highest piezoelectric constant demonstrates the highest ROS generation capability. The presence of metal/metal oxide nanoparticles on amyloid fibrils promotes the efficient separation of charge carriers under piezocatalytic conditions and increases the availability of electrons and holes to participate in redox reactions.[23] Hence, attachment of metal/metal oxide nanoparticles on amyloid fibrils enhances the piezocatalytic ROS generation. Thirdly, mechanochemically generated ROS-assisted degradation performance of rhodamine B is enhanced by 4 times after nanoparticle conjugation (Fig. 5a–d). It was found that the amyloid–Fe_3O_4 composite shows the highest rhodamine B degradation efficiency (80%) followed by the amyloid–Au composite and amyloid fibrils under similar experimental conditions. The kinetics of dye degradation can be described by a linear relationship between $\ln(C_0/C)$ and ultrasound exposure time, from which the rate constant of the degradation process can be determined (Fig. 5d). The rate constant values for the degradation of rhodamine B are 0.004 min^{-1}, 0.01 min^{-1} and 0.016 min^{-1} for amyloid fibrils, amyloid–Au and amyloid–Fe_3O_4, respectively (Fig. 5d). This result suggests that rhodamine B degradation is 4 times faster after Fe_3O_4 conjugation on amyloid fibrils. The observed mechanochemical dye degradation performance is comparable with reported piezocatalytic and photocatalytic performances[30–37] (see ESI, Table S1†).

Electron spin resonance (ESR) spectra are further recorded to confirm the formation of ROS by amyloid–Fe_3O_4 under ultrasound exposure (Fig. 6a and b). 5,5-Dimethyl-1-pyrroline N-oxide (DMPO) is used as a spin-trapping agent for detecting the hydroxyl ($^{\bullet}OH$) and superoxide ($O_2^{\bullet-}$) radicals. We have observed the four characteristic signature peaks (1 : 1 : 1 : 1) of the DMPO-$O_2^{\bullet-}$ adduct in a DMSO solvent and the four characteristic signature peaks (1 : 2 : 2 : 1) of the DMPO-$^{\bullet}OH$ adduct in a water solvent. These ESR results demonstrate the formation of superoxide and hydroxyl radicals under the mechanochemical reaction conditions. Control experiments show that in the absence of ultrasound or in the absence of amyloid–Fe_3O_4 these ROS cannot be produced. We have also studied the stability of the nanocomposites after exposure to ultrasound. Fibril-bound nanoparticles are quantified using inductively coupled plasma optical emission spectrometry showing that the nanocomposites retain the content of Au/Fe even after 2 h of ultrasound exposure (ESI, Fig. S7†). TEM images also suggest that the nanocomposites retain their morphology after 2 h of ultrasound exposure (ESI, Fig. S8†). These results suggest that the binding of Au/Fe_3O_4 nanoparticles to amyloid fibrils is stable enough against mechanical stress.

Conclusion

We have demonstrated that nanoparticle conjugation can enhance the piezoelectric property and mechanochemical reaction performance of amyloid/protein fibrils by 2–4 times. In particular, we have shown that the piezoelectric constant of nanoparticle-conjugated lysozyme fibrils can be as high as 82 pm V^{-1}. Thin films derived from these materials can generate periodic voltage/current pulses under exposure of medical grade ultrasound that can reach up to 1 V/15 nA. Ultrasound exposure of a colloidal dispersion of these materials generates ROS *via* mechanochemical reaction and degrades a dye. Although ROS can be generated by iron oxide in the presence of hydrogen peroxide,[38,39] the present approach offers an advantage in that ROS can be generated in the presence of oxygen and water and in the absence of any hydrogen peroxide. This strategy can be adapted to improve the mechanochemical reaction performance of weakly piezoelectric materials.

The observed piezoelectricity of amyloid fibrils has intriguing physiological implications considering the reported mechanical and electrical influence on these protein structures.[40–42] In particular, the piezoelectric properties of amyloid fibrils open up possibilities for therapeutic interventions. For example, external mechanical or electrical stimuli could be used to modulate their behavior or to break them down, potentially preventing their accumulation in tissues.[41,42] Given the broad range of biomedical applications for piezoelectric materials, such as wireless activation of neuronal cells,[43] cell differentiation,[44] electroporation[45] and tumor/cell therapy,[46] these piezoelectric fibril composites could be developed for similar uses.

Data availability

The data supporting this article have been included as part of the ESI.†

Conflicts of interest

The authors declare no competing financial interests.

Acknowledgements

References

1 Z. L. Wang and J. Song, *Science*, 2006, **312**(5771), 242–246.

2 X. Wang, J. Song, J. Liu and Z. L. Wang, *Science*, 2007, **316**, 102–105.

3 S. Li, Z. Zhao, J. Zhao, Z. Zhang, X. Li and J. Zhang, *ACS Appl. Nano Mater.*, 2020, **3**, 1063–1079.

4 S. D. Mahapatra, P. C. Mohapatra, A. I. Aria, G. Christie, Y. K. Mishra, S. Hofmann and V. K. Thakur, *Adv. Sci.*, 2021, **8**, 2100864.

5 A. Cafarelli, A. Marino, L. Vannozzi, J. Puigmartí-Luis, S. Pané, G. Ciofani and L. Ricotti, *ACS Nano*, 2021, **15**, 11066–11086.

6 J. Dolai, A. Biswas and N. R. Jana, *ACS Appl. Nano Mater.*, 2022, **5**, 14038–14050.

7 J. Ouyang, Z. Tang, N. Farokhzad, N. Kong, N. Y. Kim, C. Feng, S. Blake, Y. Xiao, C. Liu, T. Xie and W. Tao, *Nano Today*, 2020, **35**, 100949.

8 D. Kim, S. A. Han, J. H. Kim, J.-H. Lee, S.-W. Kim and S.-W. Lee, *Adv. Mater.*, 2020, **32**, 1906989.

9 R. Wang, J. Sui and X. Wang, *ACS Nano*, 2022, **16**, 17708–17728.

10 S. Chen, X. Tong, Y. Huo, S. Liu, Y. Yin, M.-L. Tan, K. Cai and W. Ji, *Adv. Mater.*, 2024, 2406192.

11 E. Fukada, *Wood Sci. Technol.*, 1968, **2**(4), 299–307.

12 C. A. L. Bassett and R. O. Becker, *Science*, 1962, **137**, 1063–1064.

13 H. Athenstaedt, H. Claussen and D. Schaper, *Science*, 1982, **216**, 1018–1020.

14 W. S. Williams and L. Breger, *J. Biomech.*, 1975, **8**(6), 407–413.

15 E. Fukada and Y. Ando, *J. Polym. Sci., Part B: Polym. Phys.*, 1972, **10**, 565–567.

16 M. Minary-Jolandan and M.-F. Yu, *ACS Nano*, 2009, **3**, 1859–1863.

17 K. Ryan, J. Beirne, G. Redmond, J. I. Kilpatrick, J. Guyonnet, N.-V. Buchete, A. L. Kholkin and B. J. Rodriguez, *ACS Appl. Mater. Interfaces*, 2015, **7**, 12702–12707.

18 J. Dolai, A. Maity, B. Mukherjee, R. Ray and N. R. Jana, *ACS Appl. Mater. Interfaces*, 2024, **16**(1), 217–227.

19 T. Kurita, T. Terabayashi, S. Kimura, K. Numata and H. Uji, *Biomacromolecules*, 2021, **22**(7), 2815–2821.

20 W. Qi, Y. Fu, E. Liu, Z. Cheng, Y. Sun, S. Liu and M. Yang, *EES Catal.*, 2024, **2**(4), 884–910.

21 J. Dolai, A. R. Sarkar, S. Das and N. R. Jana, *Part. Part. Syst. Charact.*, 2023, **40**(12), 2300065.

22 S. Asgari, G. Mohammadi Ziarani, A. Badiei and S. Iravani, *Mater. Adv.*, 2023, **4**(23), 6092–6117.

23 J. Dolai, A. Biswas, R. Ray and N. R. Jana, *ACS Appl. Mater. Interfaces*, 2022, **14**, 26443–26454.

24 X. Zhou, B. Shen, A. Lyubartsev, J. Zhai and N. Hedin, *Nano Energy*, 2022, **96**, 107141.

25 K. Debnath, A. K. Sarkar, N. R. Jana and N. R. Jana, *Acc. Mater. Res.*, 2022, **3**, 54–66.

26 N. R. Jana, P. K. Patra, A. Saha, S. K. Basiruddin and N. Pradhan, *J. Phys. Chem. C*, 2009, **113**, 21484–21492.

27 V. Subramanian, E. E. Wolf and P. V. Kamat, *J. Am. Chem. Soc.*, 2004, **126**, 4943–4950.

28 S. Pal and N. R. Jana, *ACS Appl. Nano Mater.*, 2020, **3**(2), 1683–1692.

29 L. Cai, J. Du, F. Han, T. Shi, H. Zhang, Y. Lu, S. Long, W. Sun, J. Fan and X. Peng, *ACS Nano*, 2023, **17**(8), 7901–7910.

30 C. Porwal, M. Sharma, R. Vaish and V. S. Chauhan, *ACS Appl. Eng. Mater.*, 2023, **1**(1), 295–303.

31 A. Shukla, A. Gaur, S. Dubey and R. Vaish, *RSC Mechanochem.*, 2024, **1**, 465–476.

32 A. Biswas, S. Saha, S. Pal and N. R. Jana, *ACS Appl. Mater. Interfaces*, 2020, **12**(43), 48363–48370.

33 M. Ismail, Z. Wu, L. Zhang, J. Ma, Y. Jia, Y. Hu and Y. Wang, *Chemosphere*, 2019, **228**, 212–218.

34 A. Mehrehjedy, P. Kumar, Z. Ahmad, P. Jankoski, A. S. Kshirsagar, J. D. Azoulay, X. He, M. K. Gangishetty, T. D. Clemons, X. Gu, W. Miao and S. Guo, *ACS Omega*, 2024, **9**, 49239–49248.

35 H. Lu, L. Zhang, J. Ma, N. Alam, X. Zhou and Y. Ni, *Nanomaterials*, 2019, **9**(2), 277.

36 Y. Zhou, J. Shen, Y. Bai, T. Li and G. Xue, *Int. J. Biol. Macromol.*, 2020, **152**, 242–249.

37 E. Ravelo-Nieto, S. A. Ovalle-Serrano, E. A. Gutiérrez-Pineda, C. Blanco-Tirado and M. Y. Combariza, *J. Environ. Chem. Eng.*, 2023, **11**, 109516.

38 K. Zhang, Z. Yang, X. Meng, Y. Cao, Y. Zhang, W. Dai, H. Lu, Z. Yu, H. Dong and X. Zhang, *Mater. Chem. Front.*, 2018, **2**, 1184–1194.

39 N. Jaafarzadeh, A. Takdastan, S. Jorfi, F. Ghanbari, M. Ahmadi and G. Barzegar, *J. Mol. Liq.*, 2018, **256**, 462–470.

40 A. Kozell, D. Eliaz, A. Solomonov, D. Benyamin, G. Shmul, O. Brookstein, I. Rosenhek-Goldian, U. Raviv and U. Shimanovich, *Proc. Nat. Acad. Sci.*, 2023, **120**, e2212849120.

41 S. Kalita, H. Bergman, K. D. Dubey and S. Shaik, *J. Am. Chem. Soc.*, 2023, **145**(6), 3543–3553.

42 I. Rosales, L. Salazar, D. Luna, A. Negrón, I. Bdikin, B. Rodriguez and A. Heredia, *Am. J. Mol. Biol.*, 2021, **11**, 1–14.

43 A. Marino, S. Arai, Y. Hou, E. Sinibaldi, M. Pellegrino, Y.-T. Chang, B. Mazzolai, V. Mattoli, M. Suzuki and G. Ciofani, *ACS Nano*, 2015, **9**, 7678–7689.

44 G. G. Genchi, L. Ceseracciu, A. Marino, M. Labardi, S. Marras, F. Pignatelli, L. Bruschini, V. Mattoli and G. Ciofani, *Adv. Healthcare Mater.*, 2016, **5**, 1808–1820.

45 J. Dolai, A. R. Sarkar, A. Maity, B. Mukherjee and N. R. Jana, *ACS Appl. Mater. Interfaces*, 2023, **15**(51), 59155–59164.

46 P. Zhu, Y. Chen and J. Shi, *Adv. Mater.*, 2020, **32**, 2001976.